J. Phys.: Condens. Matter 9 (1997) 8065–8073. Printed in the UK PII: S0953-8984(97)82026-7

The Hall effect of an inhomogeneous magnetic field in mesoscopic structures

Xin-Qi Li†, F M Peeters‡ and A K Geim§

† Institute of Industrial Science, University of Tokyo, 7-22-1 Roppongi, Minato-ku, Tokyo 106, Japan

‡ Department of Physics, University of Antwerp (UIA), B-2610 Antwerpen, Belgium

§ Research Institute for Materials, University of Nijmegen, 6525 ED Nijmegen, The Netherlands

Received 20 February 1997, in final form 17 July 1997

Abstract. We present a simulation of the motion of electrons in a mesoscopic Hall bar, scattered by a local inhomogeneous magnetic field. In the low-field regime, the Hall resistance is found to be determined precisely by the average magnetic field in the cross junction, which implies a valuable device application of non-invasive access for measuring magnetic flux, like SQUIDs do, but on a rather small (submicron) scale. The bending resistance is found to depend sensitively on the local magnetic field profile, which may also imply certain device applications, such as detecting the local magnetic properties of small objects. We also discuss briefly the asymmetric effect due to non-identical leads and asymmetric location of the field profile in the cross junction.

1. Introduction

The Hall effect has been a very successful technique for obtaining information on the properties of charge carriers, e.g. the sign of the charge carriers and their density. With the improvement of the quality of the two-dimensional electron gas (2DEG), the well known phenomena of the integer quantum Hall effect (IQHE) and the fractional quantum Hall effect (FQHE) have been discovered [1], which has stimulated the progress of low-dimensional physics greatly. In recent years, with the further development of the MBE and micro-fabrication techniques, the quasi-one-dimensional (Q1D) semiconductor system has been realized. The study of the Hall effect in the Q1D system has shown a lot of interesting transport phenomena such as the quenching of the Hall resistance at low magnetic fields, the last Hall plateau, and other anomalies [2–6]. Extensive theoretical efforts have also contributed to the understanding of these novel phenomena [7–9].

Usually the Hall system is studied under a uniform magnetic field. However, the Hall problem in the presence of an inhomogeneous magnetic field has become important recently for the composite fermion theory in the FQHE [10], since for a density-modulated 2DEG, which is in the FQHE regime, the problem can be mapped onto the modulation of the magnetic field. Moreover, due to the experimental progress, various inhomogeneous magnetic fields can now be generated on a nanometre scale. For example, by using MBE growth, semiconductor materials (e.g. GaAs) can be doped with magnetic ions (e.g. Mn). Under specific growth conditions these ions conglomerate and form ferromagnetic clusters (e.g. MnAs) with controllable diameters in the range of 5–30 nm [11]. If such a magnetic particle is placed in the cross of a Hall bar, the Hall response signal can provide us with magnetic information on the particle. This is a novel technique, which provides non-invasive

0953-8984/97/388065+09$19.50

access to the magnetic properties of very small (submicron) objects of any desired form, size and material [12]. In this context, the mesoscopic Hall probes work effectively as micro-fluxmeters, similar to SQUIDs, but with an effective detection loop of only about a square micron.

In this work, we present a theoretical investigation of the magnetic response of a Hall bar device to an individual submicron magnetic sample placed in the cross junction. We noticed that in the regime of high and uniform magnetic field, the ballistic transport in a Hall bar is dominated by the quantized edge states, which lead to quantized Hall conductance. However, in the low-magnetic-field regime a classical approach developed by Beenakker and van Houten in reference [9] worked very well as regards providing an understanding of the anomalies in a Hall bar, and was in good agreement with the quantum lattice Green's function method [8]. Therefore, in the present work we will apply this classical approach, since our main interest is in the low-magnetic-field regime. Furthermore, for considering inhomogeneity of a magnetic field, which implies the absence of well defined edge states, this classical approach appears to be quite appropriate. In our model simulation, we will also assume sharp corners and hard-wall geometry for the system. The former assumption will not influence our conclusions qualitatively; see reference [12], where slightly rounded corners were considered. The Hard-wall assumption, which has been used widely even in quantum calculations, is expected to be a better approximation in the present classical computation, since a finite-height barrier is the same as a hard wall to a classical particle, provided that the barrier is higher than the particle's kinetic energy.

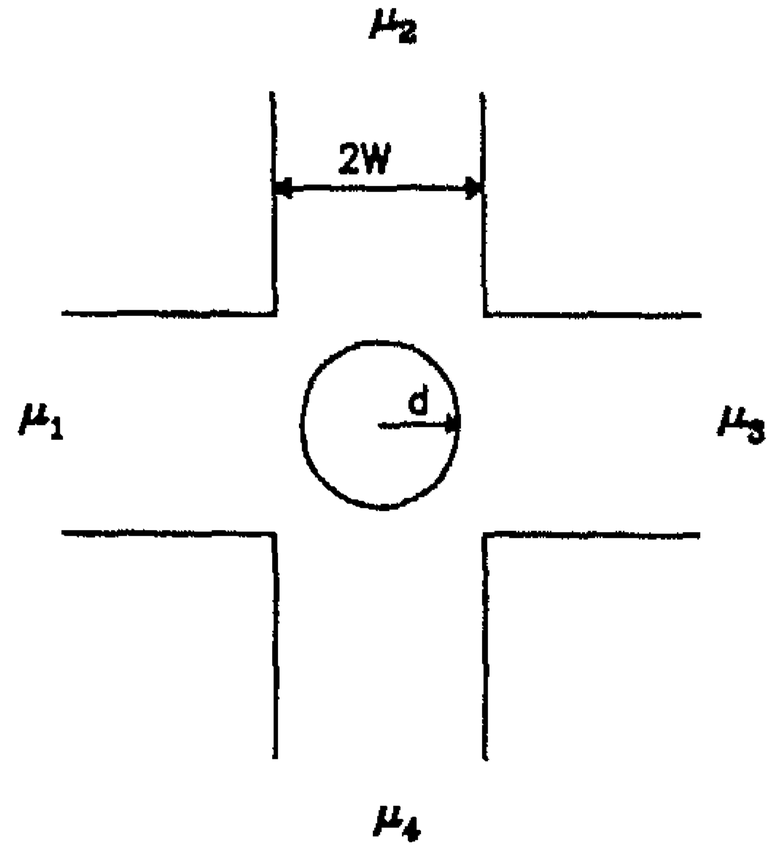

Figure 1. The four-terminal Hall bar, where an inhomogeneous magnetic field is present, which is circularly symmetric and is placed at the centre of the cross junction.

2. The model and formalism

The four-terminal geometry for the Hall measurement is shown schematically in figure 1, where the four leads are connected to reservoirs each at chemical potential μ_i. Here we show the system with four identical leads and a circular magnetic field profile situated in the middle of the cross junction. In most of the present paper we will focus our discussion on this geometry; however, the effect of non-identical leads and asymmetric location of the magnetic field profile will also be discussed briefly. Three types of circular magnetic field profile are considered. First, we consider a superconducting disc placed in an external constant magnetic field above the centre of the junction. Because of the Meissner effect,

we model the field profile as zero inside a region of radius d, and constant outside it. The scattering on this profile and the consequent physical results will be studied in considerable detail. Another two magnetic field profiles will also be discussed briefly: one is that of a single magnetic dipole which is placed a distance z_0 above the cross junction in the absence of an external magnetic field; another is a magnetic flux in the centre of the cross region which we model by a Gaussian magnetic field profile.

The Hall resistance is calculated numerically using the semi-classical formalism. The current in lead i is denoted by I_i, which can be expressed according to the Landauer–Büttiker formula as [13]

$$I_i = \frac{2e}{h}\left[(N_i - R_i)\mu_i - \sum_{j\neq i} T_{ij}\mu_j\right] \tag{1}$$

where T_{ij} is the probability of transmission for an electron from lead j to lead i, and R_i the probability of reflection back into the same lead i. In practice, these probabilities are calculated at the Fermi energy ϵ_F, and satisfy $\sum_{j\neq i} T_{ij} + R_i = N_i$, according to the condition for the current conservation, where N_i is the number of propagating modes in lead i. For the four-lead Hall geometry with identical leads, the Hall resistance R_H can be found from equation (1) by setting $I_1 = -I_3 = I$ and $I_2 = I_4 = 0$:

$$R_H = \frac{(\mu_2 - \mu_4)/e}{I} = \frac{h}{2e^2}\frac{T_{21}^2 - T_{41}^2}{Z} \tag{2}$$

and the bending resistance R_B by setting $I_1 = -I_2 = I$ and $I_3 = I_4 = 0$:

$$R_B = \frac{(\mu_4 - \mu_3)/e}{I} = \frac{h}{2e^2}\frac{T_{31}^2 - T_{41}T_{21}}{Z} \tag{3}$$

where $Z = [T_{21}^2 + T_{41}^2 + 2T_{31}(T_{31} + T_{21} + T_{41})](T_{21} + T_{41})$. For the asymmetric Hall system with either non-identical leads or an asymmetric magnetic field in the cross junction, the simple formulae (2) and (3) break down. In this case, the Hall resistance and bending resistance should be solved from equation (1) by setting the same boundary conditions for the currents as in deriving equations (2) and (3).

To obtain the probabilities T_{ij} and R_i, we follow the semi-classical approach developed by Beenakker and van Houten in reference [9]. In our numerical simulation, we inject a large number of electrons ($N_e \geqslant 10^5$) towards the junction through lead 1, and follow their classical trajectories to determine the probabilities: $T_{j1} = N_j/N_e$, where N_j is the number of electrons collected in lead j. Note that for the case of non-identical leads or an asymmetric magnetic field profile, similar procedures should be followed for each of the four leads. The electrons are injected uniformly over lead 1, with the Fermi velocity $v_F = \sqrt{2m\epsilon_F}$, and an angular distribution $P(\theta) = \frac{1}{2}\cos\theta$, where $\theta \in (-\pi/2,\ \pi/2)$ is the injecting angle with respect to the channel axis. Here the angular distribution weight function $P(\theta) \sim \cos\theta$ simply results from the slight shift of the Fermi surface of the reservoirs in the linear response regime. The factor 1/2 is from the normalization condition.

3. Results and discussion

In the following we express the magnetic field in units of $B_0 = mv_F/2eW$, and the resistance in $R_0 = (h/2e^2)\pi/2k_FW$, where W is the half-width of the lead, m the mass of the electron, $k_F = \sqrt{2m\epsilon_F/\hbar^2}$ the Fermi wave vector, and $v_F = \hbar k_F/m$ the Fermi velocity. For electrons moving in GaAs ($m = 0.067m_e$) and for a typical channel width of $2W = 1$ μm and a Fermi energy of $\epsilon_F = 10$ meV, we obtain $B_0 = 0.087$ T and $R_0 = 0.308$ kΩ.

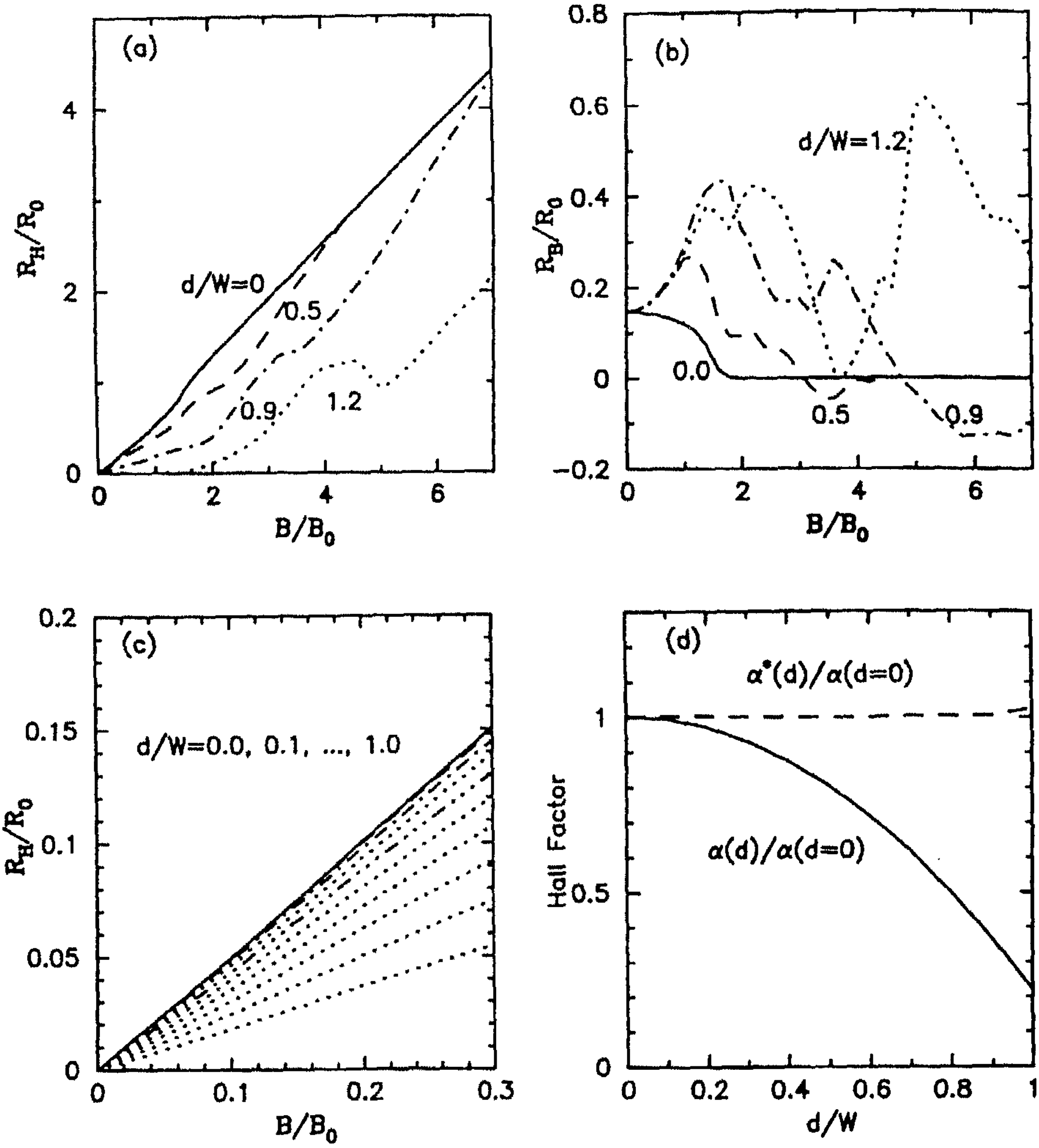

Figure 2. (a), (b) Hall and bending resistances in the presence of a superconducting disc in the cross junction, where the results for different sizes of the disc are shown. (c) The linear behaviour of the Hall resistance in the low-magnetic-field regime. (d) The Hall coefficient $\alpha = R_H/B$ (solid curve) and $\alpha^* = R_H/\langle B\rangle$ (dashed curve) as functions of the disc radius, where $\langle B\rangle$ is the average magnetic field in the cross junction.

First, in figure 2 we present the results from the superconducting disc above the symmetric junction. In figure 2(a) we show the Hall resistance as a function of the external applied magnetic field for different sizes of the disc. Notice that there exists a critical magnetic field B_c, such that when $B > B_c$ the Hall resistance in the presence of the disc coincides with that for the case of a homogeneous magnetic field (i.e. $d = 0$). When $B < B_c$ the Hall resistance is influenced by the presence of the disc. This critical magnetic field B_c is determined by the condition that at this value the diameter of the cyclotron orbit equals the distance between the edge of the dot and the corner of the cross junction. Therefore, for $B > B_c$, the motion of an electron is described by the skipping orbits which are located along the edge of the device, and do not sense the $B = 0$ region in the cross junction,

and consequently give rise to a Hall resistance exactly the same as the classical 2D value $R_H = 2B/\pi$, which is also in the reduced units of R_0 and B_0, for both the presence and the absence of a superconducting disc above the Hall bar system. For $B < B_c$, the electron orbits are not strongly bent, so they move through the $B = 0$ region in the junction. This results in the following behaviour of the Hall resistance: there is a shoulder for a small dot, and it changes eventually to a rounded peak with increasing size of the dot. This feature can be understood as follows: with increasing magnetic field, the difference between the transmission probabilities T_{21} and T_{41} increases first, and then decreases when the magnetic field is larger than a certain critical value. On the other hand, the quantity Z in equation (2) is a monotonically decreasing function of magnetic field. Thus, a shoulder or rounded peak as in figure 2(a) occurs at around the maximum point of $T_{21} - T_{41}$. This is also the reason for the non-linear behaviour in the intermediate region between the low and high magnetic fields in the absence of the superconducting dot (see the solid line in figure 2(a)), which connects the two linear regimes with different slopes.

In figure 2(b) the bending resistance is shown. The non-zero value of the bending resistance is a quite interesting feature of a mesoscopic Hall bar system, since for a macroscopic ohmic structure, two leads attached to the same point on the current path measure nearly the same voltage, so $R_B \sim 0$. From figure 2(b), for the case of $d = 0$, we find a non-zero bending resistance in the low-magnetic-field regime. With increasing magnetic field, R_B decreases, and becomes zero after $B \geqslant 2B_0$, which is in the classical 2D regime, where, in addition to the classical 2D Hall resistance, this zero bending resistance is expected. Therefore, here the zero bending resistance and the classical 2D Hall resistance reflect in an interesting way the fact that the magnetic field changes the system from the mesoscopic to the macroscopic regime. In the presence of a superconducting dot, we find that the behaviour of the bending resistance is quite different from the $d = 0$ case. In the low-magnetic-field limit, in addition to the geometry scattering, the scattering on the superconducting dot destroys the guiding of the magnetic field, and thus the bending resistance increases with increasing magnetic field. However, after the magnetic field has gone beyond certain critical value, which is proportional to the size of the dot, the guiding dominates the motion of electrons, and the bending resistance decreases with the magnetic field. We notice that, for a large size of the dot, the bending resistance exhibits further oscillation with increasing magnetic field. The region of increasing R_B corresponds to the region of decreasing R_H, and vice versa. This feature is intuitively reasonable, since the stronger bending of the field towards the direction of motion of the electrons results in a larger Hall voltage, but a smaller bending voltage due to the better guiding of the motion along the current path. We also observe a sign reversal in R_B, which is due to the incomplete guiding, at fields where R_H is rapidly rising. Here, the main but somewhat complex structures of the bending resistance in figure 2(b) correspond exactly to the relatively smooth behaviours of the Hall resistance in figure 2(a), both of which are computed from the same data for T_{ij} by using equations (2) and (3), and can be understood quite physically. However, we are not very sure of the origin of the small structures in the bending resistance, which may result from the numerical accuracy limitation, although the accuracy has been examined carefully by changing the numbers and initial positions and directions of the injected particles for the Hall resistance in figure 2(a), and may not be so high for the bending resistance, due to its more sensitive dependence on the magnetic field profile in the cross junction. In this context, we point out that the bending resistance may be an important quantity in mesoscopic Hall measurement, because of its high sensitivity to the local magnetic field in the cross junction, which may lead to some useful techniques for detecting a local magnetization in the cross.

Note that, even in the presence of the disc, the behaviour of the Hall resistance for low magnetic fields is linear—see figure 2(c), where the slope decreases with the disc size, i.e. with the amount of the expelled magnetic flux. In this context, it is helpful for us to analyse the Hall coefficient $\alpha = R_H/B$. In figure 2(d), we show that the Hall coefficient decreases with increasing radius of the disc (see the solid curve), because of the reduction of the average magnetic field in the cross junction. Furthermore, if we use the average field $\langle B \rangle$ in the cross junction, $\langle B \rangle = [1 - \pi(d/2W)^2]B$, to define an effective Hall coefficient as $\alpha^* = R_H/\langle B \rangle$, we find that α^* is independent of d for $d/W < 1.0$, which is shown by the dashed curve in figure 2(d). For $d > W$, where only in the small regions near the four corners is the magnetic field non-zero, our simulation gives a decreasing behaviour for α^* with the further increase of d. This breakdown is due to the ineffective scattering of the *extremely corner-located* magnetic field of the electrons. However, the remarkable result of constant α^* in figure 2(d) indicates that in low-magnetic-field regime the Hall resistance is determined completely by the average field in the cross region, and is independent of the detailed distribution of the field. This is one of our major conclusions in this work, which will be confirmed further in the following by investigating other inhomogeneous magnetic field profiles.

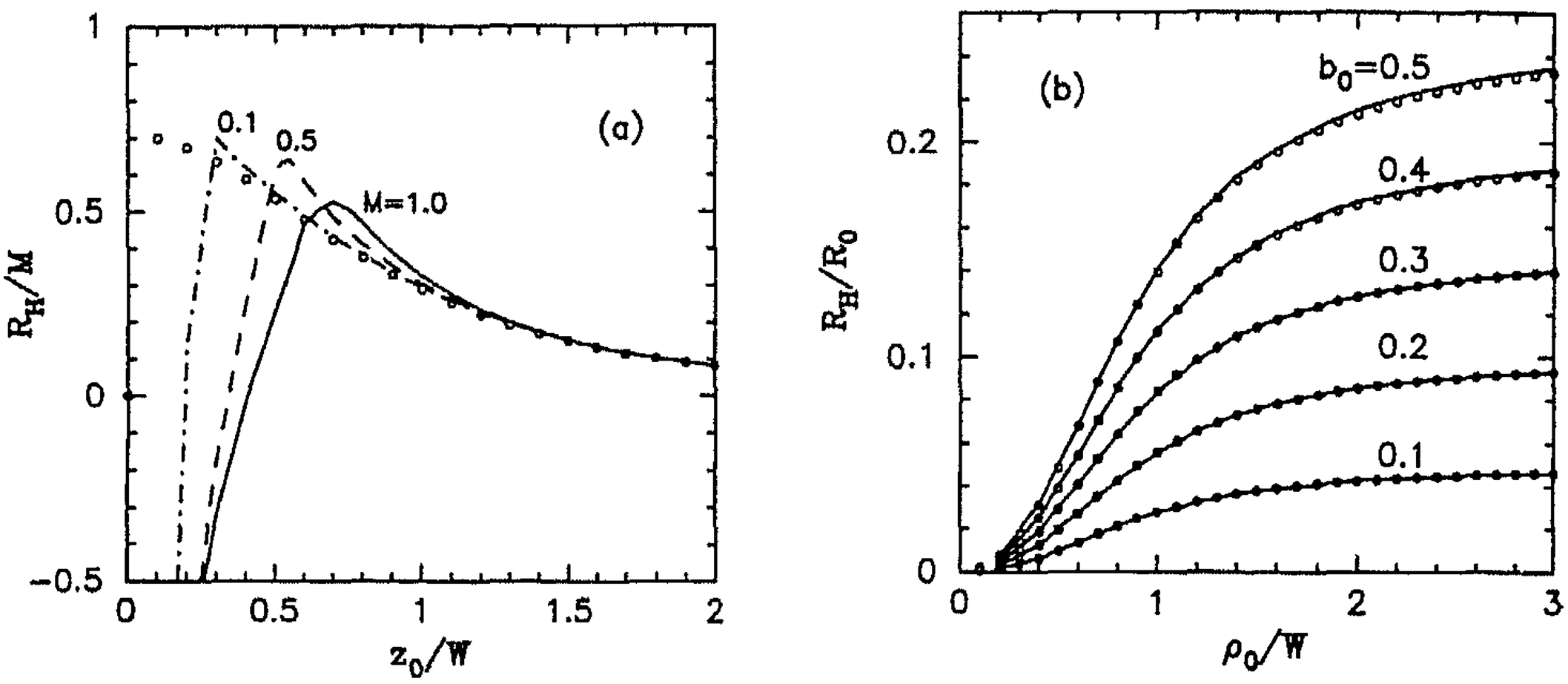

Figure 3. The Hall resistance from (a) a magnetic dipole, and (b) a magnetic vortex in the absence of an external magnetic field, where the small circles are obtained from $R_H = \langle B \rangle/2$.

With this aim, we consider the scattering by another two types of magnetic field profile, namely a magnetic dipole and magnetic flux, in the absence of other external magnetic fields. First, for the magnetic dipole, the component of the magnetic field perpendicular to the 2D plane is given by $B(\rho) = M(3\cos^2\theta - 1)/R^3$, where $R^2 = \rho^2 + z_0^2 = x^2 + y^2 + z_0^2$, $\cos^2\theta = z_0^2/R^2$, z_0 is the distance between the dipole and the 2D plane, and M is the dipole moment. In figure 3(a) we show the scaled Hall resistance R_H/M as a function of the distance z_0. The results for $M = 1$, 0.5, and 0.1 are given by the solid, dashed, and chain curves respectively. We see that for large z_0, the Hall resistance R_H scales perfectly with M. This feature proves that the Hall resistance is proportional to the average magnetic field over the junction region in low-field limit. In figure 3(a) we also present the result obtained from $R_H = \langle B \rangle/2$, shown by the small circles, where we see clearly that this simple formula can give exactly the same result as is obtained from the numerical simulation. However, with decreasing z_0, the Hall resistance deviates from the above simple formula, because of the more strongly non-uniform magnetic field. For small z_0, $B(\rho)$ has a sharp positive core

at the centre which is not sensed by the electrons; consequently a negative Hall resistance appears in this regime.

Next, for the magnetic flux, we model it by a Gaussian magnetic field profile $B(\rho) = b_0 \exp(-\rho^2/\rho_0^2)$, where $\rho = \sqrt{x^2 + y^2}$, ρ_0 describes the spread of the magnetic field, and b_0 describes the strength of the field. In figure 3(b) we show the Hall resistance as a function of the width ρ_0 of the magnetic field profile, for several values of the strength. The solid lines are for the results from the numerical simulation, and the small circles are for those obtained from the formula $R_H = \langle B \rangle/2$. Here we illustrate again that in low-magnetic-field regime the Hall resistance is determined precisely by the average magnetic field in the cross junction, and is independent of the detailed distribution of the field.

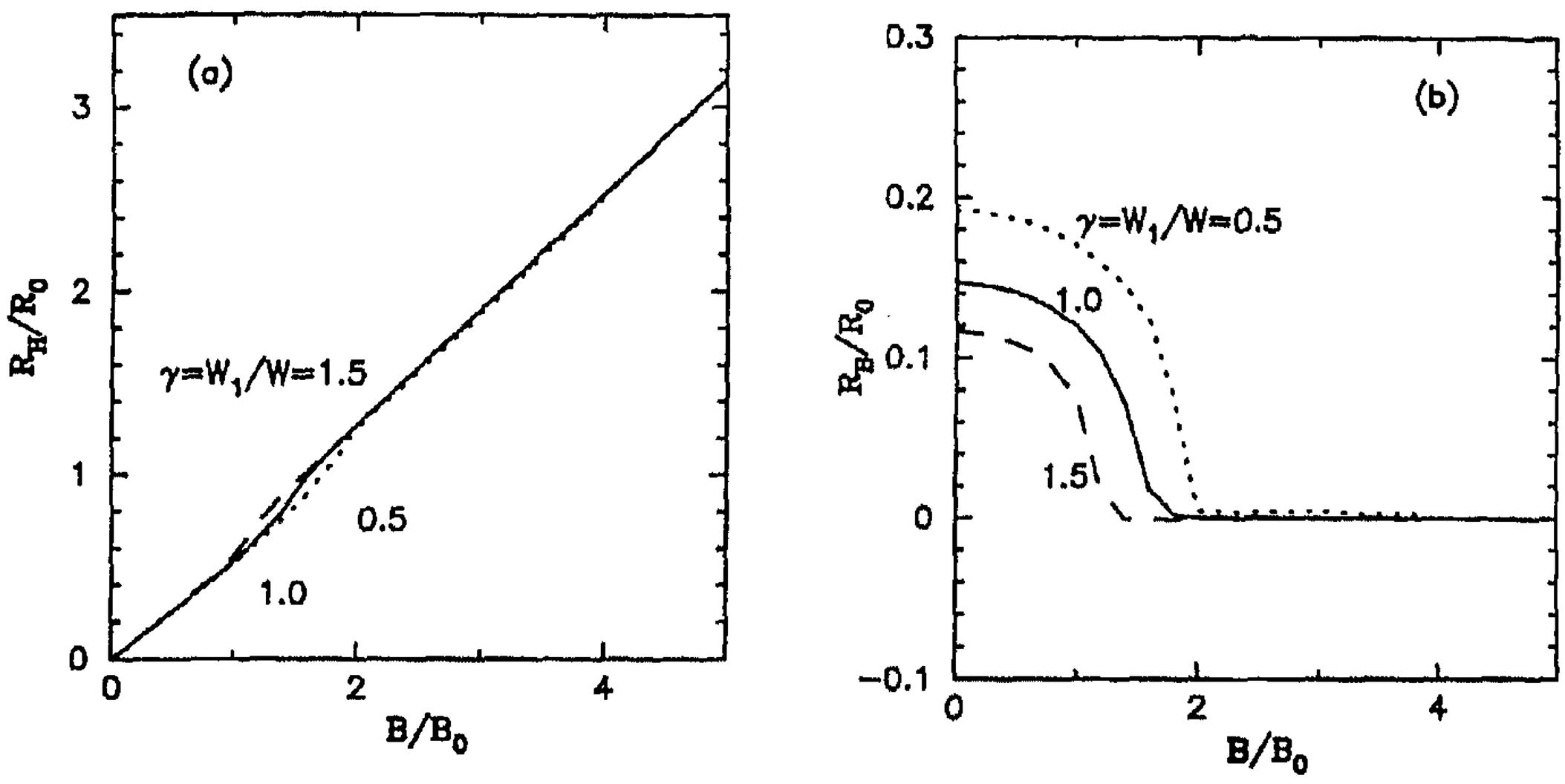

Figure 4. The Hall resistance (a) and bending resistance (b) for an asymmetric Hall bar. The width ratio of two pairs of leads is denoted by $\gamma = W_1/W$ (see the text for a more detailed description).

The above discussions are restricted to the symmetric systems. To show the asymmetric effects on the Hall and bending resistances, let us consider the asymmetric system with non-identical leads, for the specific case of a homogeneous magnetic field. To be definite, we denote the ratio of the widths of lead 2 (4) and lead 1 (3) (see figure 1) by $\gamma = W_1/W$. The results are shown in figures 4(a) and 4(b) for $\gamma = 0.5$ (dotted curve), 1.0 (solid curve), and 1.5 (dashed curve).

(1) In the high-magnetic-field regime, the Hall resistances overlap with each other precisely, and have the classical 2D value. Meanwhile, the bending resistance is zero. This is simply the classical 2D regime.

(2) There exists an intermediate regime for each case, where both the Hall resistance and the bending resistance depend on the geometry—namely, the ratio γ. For the case of $W_1 < W$, the critical field B_c for the transition to the classical 2D system is larger than that for $W_1 = W$. For $W_1 > W$, the result is the opposite.

(3) In the low-magnetic-field regime, the Hall resistances again become the same for different values of γ, while the bending resistances are quite different from each other.

The bending resistance, including its behaviour in the intermediate regime, can be understood as follows. Since the current flows from lead 1 to lead 2, the voltage measured between lead 3 and lead 4 would decrease with increasing width W_1, because the geometry scattering is weaker for the current flowing into a wider lead than in the opposite case.

Another type of asymmetry is the asymmetric location of the circular magnetic field profile in the cross junction. In the low-magnetic-field regime, we found that the Hall resistance is still determined exactly by the average magnetic field in the cross junction, but the bending resistance depends on the location of the field profile sensitively. In the intermediate regime, both the Hall and bending resistances are influenced by the location of the magnetic field profile. In the high-field regime, in particular for the system with a superconducting disc studied above, a pure 2D classical feature is approached after the magnetic field goes beyond a certain value, which depends on the size and location of the disc.

4. Conclusions

In summary, we have applied a semi-classical approach to simulate the motion of electrons in a mesoscopic Hall bar, in the presence of an inhomogeneous magnetic field resulting from (1) a superconducting dot, (2) a magnetic dipole, and (3) a magnetic vortex. We found that in the low-magnetic-field regime the Hall resistance is determined completely by the average magnetic field in the cross junction of the Hall bar and is independent of the shape of the field profile. This finding may imply a novel technique which provides non-invasive access to magnetic properties over a very small scale—namely, systems working effectively as micro-fluxmeters similar to SQUIDs, but with an effective detection loop of only about a square micron. For the bending resistance, we showed its sensitive dependence on the magnetic field profile in the cross junction, which may in practice be helpful for detecting the inhomogeneity of the magnetic field effectively. However, because of its complicated manner of dependence on the field profile, further work to determine their relation is required, for various types of inhomogeneous magnetic field profile. We also discussed briefly the asymmetric effect on the Hall and bending resistances, due to the device geometry and asymmetric location of the circular inhomogeneous magnetic field profile. Finally, we mention that the present approach is essentially a classical method, which worked very well in the low-magnetic-field regime [8, 9]. Consequently, our results in the high-magnetic-field regime should be understood on the classical level, where we found a transition to classical 2D behaviour when the magnetic field goes beyond certain critical value.

References

[1] For a recent review see, e.g.,
Chakraborty T and Pietiläinen P (ed) 1995 *The Quantum Hall Effects* (Berlin: Springer)

[2] Roukes M L, Scherer A, Allen S J, Craighead H G, Ruthen R M, Beebe E D and Harbison J P 1987 *Phys. Rev. Lett.* **59** 3011

[3] Ford C J B, Thornton T J, Newbury R, Pepper M, Ahmed H, Peacock D C, Ritchie D A, Frost J E F and Jones G A C 1988 *Phys. Rev.* B **38** 8518

[4] Timp G, Chang A M, Mankiewich P M, Behringer R, Cunningham J E, Chang T Y and Howard R E 1987 *Phys. Rev. Lett.* **59** 732
Timp G, Baranger H U, deVegvar P, Cunningham J E, Howard R E, Behringer R and Mankiewich P M 1988 *Phys. Rev. Lett.* **60** 2081

[5] Simons J A, Tsui D C and Weimann G 1988 *Surf. Sci.* **196** 81

[6] Chang A M, Chang T Y and Baranger H U 1989 *Phys. Rev. Lett.* **63** 996

[7] Peeters F M 1988 *Phys. Rev. Lett.* **61** 589
Kirczenow G 1989 *Phys. Rev. Lett.* **62** 2993
Akera H and Ando T 1989 *Phys. Rev.* B **39** 5508

[8] Baranger H U and Stone A D 1989 *Phys. Rev. Lett.* **63** 414

Baranger H U, DiVincenzo D P, Jalabert R A and Stone A D 1991 *Phys. Rev.* B **44** 10 637
[9] Beenakker C W J and van Houten H 1989 *Phys. Rev. Lett.* **63** 1857
[10] Halperin B I, Lee P A and Read N 1993 *Phys. Rev.* B **47** 7312
Kim Y B, Furusaki A, Wen X G and Lee P A 1994 *Phys. Rev.* B **50** 17 917
Kim Y B, Lee P A, Wen X G and Stamp P C E 1995 *Phys. Rev.* B **51** 10 779
Jain J K 1989 *Phys. Rev. Lett.* **63** 199
[11] De Boeck J, Oesterholt R, Van Esch A, Bender H, Bruynseraede C, Van Hoof C and Borghs G 1996 *Appl. Phys. Lett.* **68** 2744
[12] Geim A K, Dubonov S V, Grigorieva I V, Lok J G S, Maan J C, Li X Q, Peeters F M and Nazarov Yu V 1997 *Superlatt. Microstruct.* at press
[13] Büttiker M 1986 *Phys. Rev. Lett.* **57** 1761